ARMA 24-448

Micro-seismic Monitoring in Mines Benefits and Limitations

Rebuli, D.B.
Institute of Mine Seismology, Ottawa, Ontario, Canada

ABSTRACT: Seismic monitoring is a useful tool in understanding the rockmass response to mining. The waveforms recorded by sensors contain information not only about where and when a seismic event occurred but also about the driving stresses, failure mechanism and the intervening rockmass. It is also good to understand the limitations of this tool as they should guide the system design, overall monitoring objectives and the analysis of the seismic data. This paper discusses what information can be extracted from a mine seismic system, how this information can be useful to the mine in understanding their rockmass interaction with mining, but also the limitations associated with this information. Only then can the data be interpreted correctly.

1 INTRODUCTION

Seismic monitoring in a mining environment is a unique tool, in that it is continuous in time and can monitor a 3D volume. It is also a powerful tool, in that it can monitor ground motions over multiple orders of magnitude. For example, in the velocity domain, the sensors can measure ground motions from fractions of $\mu m/s$ to tens of mm/s. The commonly used magnitude scales, which are logarithmic scales, typically extend from around -2.0 to $+2.5$ for mining applications, which is at least four orders of magnitude. The sources of the measured ground motions can be many and will be discussed below, but the main objective is to monitor sudden inelastic deformations as a result of stress changes in the rock mass due to mining. This gives a powerful monitoring tool, but it is still just one of many tools available to rock mechanic practitioners.

One of the first questions when contemplating or designing a seismic system should be “What is the objective?”. Mendecki et al. (1999) describes seismic monitoring as enabling the quantification of exposure to seismicity. They then list a number of specific objectives, namely location of potential rockbursts, prevention, control, warnings and back-analysis. Identifying the objectives is important, as it will determine such details as which sensors to use, how many and how dense a seismic array is needed and what type of alerts are required.

This paper will not go into too much detail about seismic monitoring systems and array design, except where needed to clarify a concept. However, a short introduction to seismic sources and sensors is useful.

1.1. Seismic sources and waves

The definition of a seismic source (Mendecki et al., 1999) is a sudden inelastic deformation of the rock mass that radiates detectable seismic waves. This is a fairly broad term, which could include blasts, impacts from machinery or falling rocks. The energy from any of these sources will radiate out into the rock mass as seismic waves, which may be recorded by the sensors.

Seismic waves fall into two broad categories, namely body waves and surface waves. Since this paper discusses seismic monitoring in mines, surface waves will not be discussed, except to note that these can be recorded on near-surface sensors. Body waves are further divided into Primary (P) waves and Secondary/Shear (S) waves. P-waves travel the fastest, while S-waves are only present in solids. Depending on the source of these waves, they may radiate out from the source in different patterns. The P- and S-wave radiation pattern from a shear source is shown in Fig. 1. From a blast or implosive source, the P-wave radiation pattern is more spherical, and in theory, little S-wave energy is radiated from these sources. The result is that by measuring the relative ground motions at locations around

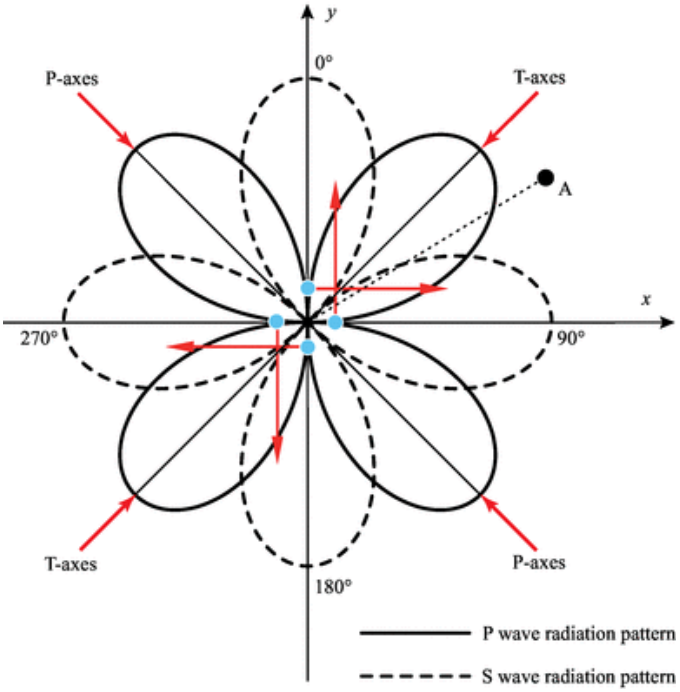

Fig. 1: Far-field radiation patterns of P- and S-waves from a shear source (from Zheng et al. (2018)).

the source, it may be possible to reconstruct the type of source. This concept is discussed in more detail later.

1.2. Seismic Sensors

There are a number of papers and books written about the various sensors used for measuring seismic waves and more details can be found in Mountfort and Mendecki (1997) and Rebuli et al. (2017), for example. Two broad sensor types are commonly used in mine seismic systems, namely miniature Geophones and Integrated Electronic PiezoElectric (IEPE) Accelerometers. IEPE accelerometers are high frequency accelerometers, with natural frequencies in the kHz range. While low frequency accelerometers do exist, these are not typically used in mine seismic systems, although there is a use-case for these for specific monitoring objectives. This is will be discussed below. For the remainder of this paper, unless specified otherwise, references to accelerometers will mean IEPE accelerometers.

While, in theory, accelerometers have a usable frequency range from around $1Hz$ up to their natural frequency, these sensors have high noise levels at low frequencies. This means they are very good at recording very small seismic events but are not so good at recording larger seismic events, especially as the distance from the source increases (Rebuli et al., 2017). Geophones do not have as high an upper frequency range as most accelerometers, but they do come close. They are also much better at low frequencies, down to their natural frequencies.

As a very broad generalization, for typical use-cases, accelerometers are good in the moment magnitude range from around -3.0 to about -1.0, while geophones are good from around -2.0 to around $+1.5$, which suggests geophones as a better all-round sensor for mine seismic systems. Accelerometers do have their advantages, and when it comes to monitoring a small volume with the objective of recording very small seismic events, these would be preferred over geophones.

For recording seismic events larger than around moment magnitude $+1.5$, more specialized sensors may be required. This is where low frequency accelerometers or broadband sensors are recommended, to properly capture low frequencies produced by these larger magnitude events.

Another aspect of seismic sensors to consider is the number of components. Three component, or triaxial, sensors have three sensor elements arranged orthogonal to each other, while single component, or uniaxial, sensors only have one sensor element. The distinguishing factor here is that uniaxial sensors will not capture the full P- and S-wave energy. In fact, depending on the orientation of the single component to the source, one of these waves may be completely missed. The advantage is that uniaxial sensors are cheaper, so more can be installed for the same cost. However, quantity over quality doesn't usually equate to a better recording system.

Good physical coupling of the sensor to the rock mass is important for quality signals. Installing sensors in boreholes which are grouted afterwards is best practice. It should be noted, installing a sensor on the surface of an excavation is not always a bad choice. It depends on the monitoring objective. If the objective is to directly measure the site effect at a sensitive underground excavation, such as a crusher station, then installing a sensor on the surface of the excavation is ideal.

2 EVENT CLASSIFICATION

As mentioned in the introduction, a seismic source is not only a sudden fracture or slip along a geological feature. The sensors record ground motions irrespective of the source and so part of the task when analyzing the recordings is to classify the type of source. The goal is to remove sources which are not directly related to the response of the rock mass due to mining. Signals from blasts are probably the easiest to identify as mines typically know when they blast, and each shot is effectively a source. The sensors would then record multiple sources within a very short time period. In fact, the seismic system can be used to monitor blasting, if there is at least one sensor at an

appropriate distance from the blast.

Other sources, such as the noise created by tipping ore or waste down a pass, are not as easily identified. One method is to exclude any source which is located close to active passes. Unfortunately this method would also exclude sources which may indicate that a pass is scaling. Research into features of waveforms, for example Meyer et al. (2022), have shown success when it comes to classifying sources and these techniques can help in "cleaning" up the data for analysis. From here on, any reference to a (seismic) event should be understood to be a seismic source which has been classified as a source associated with the response of the rock mass to mining.

3 BASIC SOURCE PARAMETERS

Seismic source parameters, such as seismic moment, M (or potency, P), radiated energy, E, and corner frequency, f_c, can be estimated from the spectral analysis of the waveforms, for each body wave. This paper will not go into the theory, however, for those interested in the details Madariaga (2015) gives a comprehensive discussion on seismic source theory. Fig. 2 shows the far-field displacement spectra for a typical seismic event, with the seismic moment being determined by the low frequency plateau of the displacement spectra. The corner frequency is the point at which the low frequency plateau and the high frequency attenuation intersect. Radiated energy is estimated by integrating the square of the spectra, in the velocity domain, after correcting for geometric spreading and frequency dependent attenuation. With source estimates relying on the sensors being in the far-field, typical source estimation code requires capturing a minimum number of wavelengths of the dominant wave. If fewer wavelengths are available, the far-field requirement may not be met and source estimates should not be calculated.

3.1. Seismic Moment

This is related to the coseismic inelastic deformation at the source. It is easier to visually understand seismic potency, which is the product of the average slip of a shear event, $\bar{u}$, and the source area, A:

$$P = \bar{u}A \tag{1}$$

Moment and potency are related by the rigidity of the rock mass around the source, μ:

$$M = \mu P \tag{2}$$

Moment, or potency, is one way to quantify the size of the seismic event, and the most commonly used magnitude scale used by seismologists is moment magnitude (see below).

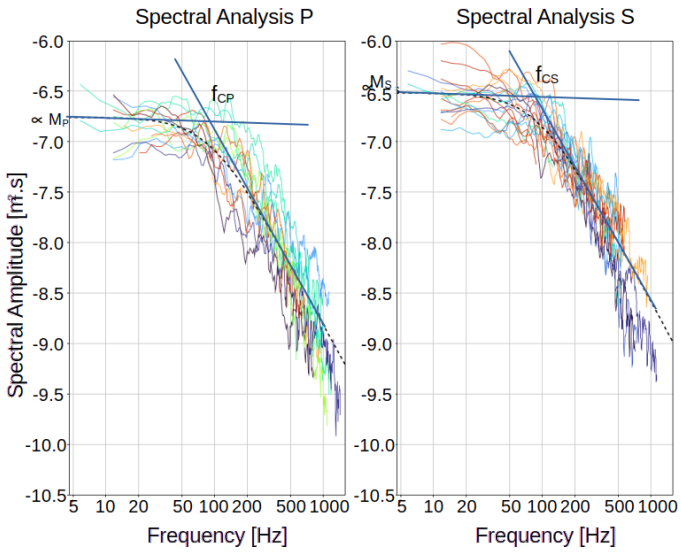

Fig. 2: Far-field displacement spectra for P- and S-waves. The low frequency plateau is proportional to seismic moment. The corner frequency (f_C) is the inflection point of the low frequency plateau and the high frequency attenuation.

Since moment is estimated from the low frequency content of the radiated seismic waves, it does not tell us anything about the source dynamics, it is a static parameter of the source.

Estimating seismic moment depends on how well the seismic sensors record frequencies below the corner frequency (Mendecki, 2013) . For smaller magnitude events (below $m_W + 1.0$), the corner frequency is large enough to fall sufficiently in the usable frequency band of a typical 14 or $15Hz$ geophone. For events with magnitudes larger than around $m_W + 1.0$, moment will start to be underestimated, as the size of the event increases. At this point, sensors able to capture lower frequencies are required. A well-installed $4.5Hz$ will increase the magnitude threshold to around $m_W + 2.0$, with events larger than this requiring a $1Hz$ geophone or broadband sensor. These low frequency sensors need to be installed at some distance from the source, usually a few km, otherwise the time separation between the P- and S-waves is not sufficient to measure the low frequency of the P-wave before the onset of the S-wave.

3.2. Radiated Seismic Energy

This is the portion of the energy radiated as seismic waves. Radiated seismic energy tells us about the dynamics of the source, for example how quickly the rupture occurred. Unfortunately, estimating the radiated energy is less accurate than estimating seismic moment, mainly due to the uncertainties in the attenuation of higher frequencies in

the rock mass between the source and the sensor. One of the factors affecting this attenuation is the rock mass quality, as a more fractured rock mass will attenuate the high frequencies faster than a more competent, homogeneous rock mass. Mendecki (2013) also discusses the limitations of estimating radiated energy depending on the usable frequency band of the sensors.

4 ANALYSIS

4.1. Ground motion

Each sensor will record the ground motion, be it velocity or acceleration, experienced at the sensor. This is a direct measurement which can give information about how a particular location in the mine responds to transient waves. Comparing sensors installed in boreholes and sensors installed on the excavation can be used to determine the amplification of the wave at the excavation. This may help with ground support design.

Ground Motion Prediction Equations (GMPE) are a common tool in ground support design for seismically active mines (Kaiser et al., 1996). If a GMPE has been calibrated for the mine, it is possible to infer the ground motions at any point in the mine as a result of a certain sized (magnitude) event at a given location. This can be used as an input to the potential for shakedown damage and for support design for this type of failure. Caution should be used when using a GMPE for locations close to a potential large event as some simple GMPE's grossly exaggerate ground motions at small distances. Once within the source of a seismic event, the ground motion is controlled, not by magnitude, but by the stress drop (Kanamori, 1972).

4.2. Event Time

The simplest and most reliable information provided by a seismic system is the time at which an event was recorded. This is useful in and of itself, especially for larger events, but when taken in conjunction with a collection of events becomes an important tool. This activity rate can help identify periods of increased seismic hazard or to better understand the baseline activity rate. Event time is also the basis for Omori's Law (Omori, 1894) which is discussed below.

4.3. Omori Analysis

Omori (1894) noted that the rate of aftershocks following a large seismic event followed a reciprocal time rate:

$$n(t) = \frac{k}{c+t} \tag{3}$$

where k and c are constants, which vary between earthquake sequences. This has become known as Omori's Law, even though it was more of an observation, and was since modified by Utsu (1961) as follows:

$$n(t) = \frac{k}{(c+t)^p} \tag{4}$$

where p falls between 0.7 and 1.5. This decay rate of aftershock activity has been observed in mine seismology, after large seismic events, and also after blasting. It has prompted people to use this relationship to determine reentry times after a large event or a production blast (Vallejos and McKinnon, 2008). The downside is that the constants need to be calibrated, and the decay rate for each large seismic event or blast depend on the local stress conditions. Re-calibration is required often and so this law is not a good practical tool for re-entry times.

4.4. Event Location

Seismic sensors record the P- and S-waves. By using the arrival times of these waves, at multiple sensors, and predetermined seismic wave velocities, the source location can be triangulated. For larger magnitude events, this is used for determining exclusion zones and where in the mine attention should be focused. For smaller events, this highlights regions in the mine where the seismic hazard may be increasing and potential areas for reevaluating the ground support.

It is important to keep in mind that event locations, as reported by the seismic system, are not points in space, but rather three dimensional regions. This is due to a couple of factors, namely that a seismic event has a volume, and there are uncertainties in determining the location.

Location uncertainty is determined by three factors, namely array geometry around the source, errors in determining the P- and S-wave arrival times, and velocity uncertainties. Anecdotally, the more sensors recording the waves from the event the more accurate the location. This is only true if the source is surrounded by sensors. If the sensors are off to one side, or all lie on a plane, this will negatively impact the location accuracy.

Determining the arrival times of the waves depends on how clearly the signal stands out from the noise, for a P-wave, and from the coda of the P-wave for the S-wave. High noise levels at a sensor, potentially due to a nearby fan, for example, will impact the accuracy of the arrival time picking. A uniaxial sensor, where the element is not aligned with the source, may also result in a small P-wave arrival, and hence less accurate arrival time picking. Sensors installed on the surface of the excavation, or in shallow boreholes, may be subject to surface amplification and noisy coda from the fractures around the excavation, mak-

ing S-wave arrival time picking difficult. Similarly, not grouting the sensor borehole would increase the noise on the sensor, after the P-wave arrival, complicating the picking of the S-wave arrival. All of these factors will contribute to the location uncertainty of the event. Uncertainties in the seismic wave velocities are another contributing factor for location uncertainty. Most of these can be addressed with good practices for sensor installation and with proper velocity calibrations.

The location algorithm used is another aspect of location accuracy. There are many location methods, for example the simple homogeneous velocity method, relative location methods, full waveform methods, methods taking into account the directions of first arrivals, and complex 3D velocity models with ray-tracing. The more complex the velocity contrasts in the rock mass the less useful a homogeneous velocity method will be. Although, caution should be used when making a complex velocity model, as mining will change this quickly. These models are also difficult to calibrate and there may be a simpler solution which will achieve similar results. One such solution is to continually make use of blasts to update a psuedo-3D velocity model using apparent adaptive velocities (Martinsson, 2012).

In stratified ground, it is difficult to create a good velocity model perpendicular to the bedding. Therefore, uncertainties in location will usually increase in the direction perpendicular to the bedding. Location uncertainties parallel to the bedding are usually easier to constrain in these environments.

4.5. Magnitude

The size of seismic events are often described by a number, referred to as magnitude. Reducing a complex process down to a single number is an oversimplification of the problem, but it does give a number to compare between seismic events. A few magnitude scales are discussed below. A common feature is that these scales are logarithmic, where values can be positive or negative.

Richter Magnitude

In the 1930's, Charles Richter (Richter, 1935) developed a method to compare the size of seismic events. This was based on the maximum amplitude of the waveform, as recorded on a specific type of seismometer, and the distance that recording was from the source. This was specific to California and became known as the Richter Scale. As more seismograph stations were installed around the world, it became apparent that the Richter Scale had a number of shortcomings. Unfortunately, this is the magnitude scale that the public think about when magnitude is mentioned in the media.

Moment Magnitude

The most commonly used scale, by seismologists, is the moment magnitude scale, m_W. Moment is a physical quantity which can be estimated from recorded waveforms, as described in Eq. 2. The standard equation for moment magnitude is (Hanks and Kanamori, 1979):

$$m_W = {}^2\!/_3 \log_{10}(M) - 6.03 \tag{5}$$

where M is the seismic moment. The equation was designed to match the Richter Scale for smaller magnitudes. The range of moment magnitudes typically recorded in mines is between -2.5 and $+2.5$. Larger magnitude events can occur in mines, but are rare. Smaller events do occur, but these are more difficult to record with typical sensors used in mine seismic systems. To put this into perspective, a shear crack of a few *cm* would be equivalent to a $m_W - 2.0$ event, while movement on a fault, about $200\,m$ in length, would be the equivalent of around $m_W + 2.0$. The maximum displacement on that fault may only be a few *cm*.

Nuttli Magnitude

Eastern Canada uses the Nuttli magnitude scale (m_N). This is based on the amplitude of a particular surface wave. This wave is not recorded by in-mine seismic systems, but mines in Eastern Canada are typically asked to report using this magnitude scale. An empirical relation between m_W and m_N was proposed by Sonley and Atkinson (2005):

$$m_W = 1.03 m_N - 0.61 \tag{6}$$

4.6. Frequency-magnitude distribution

Plotting the cumulative number of events above a certain magnitude vs magnitude yields a plot as shown in Fig. 3. This is typically modeled by Eq. 7 as proposed by Gutenberg and Richter (1944):

$$\log N(\geq m) = a - bm \tag{7}$$

where $N(\geq m)$ is the expected number of events not smaller than magnitude m, and a and b are constants. The slope of the line, b, is typically around 1.0 for regional seismicity. In mining, b can vary quite significantly from 1.0. El-Isa and Eaton (2014) looked at variations in b for catalogues of seismicity for the whole earth and concluded that variations in b were related to changes in effective stress. Other work using crustal seismicity has tried to link temporal variations in b with changes in seismic hazard (El-Isa, 2018).

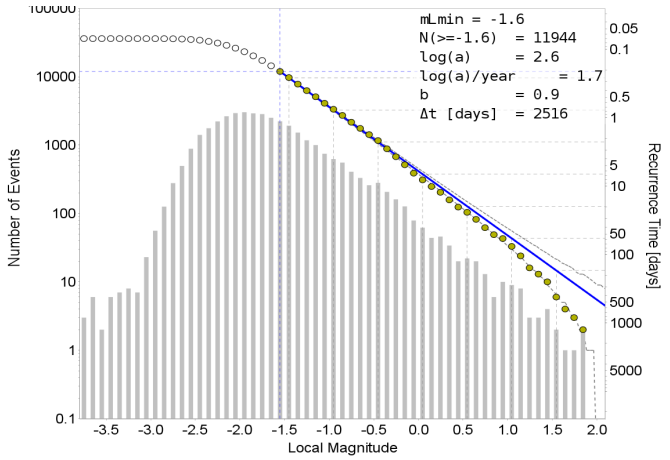

Fig. 3: Frequency-magnitude plot showing the cumulative number of events (circles) vs magnitude, for a 7 year time period. The bars indicate the number of events per magnitude bin, with the magnitude associated with the peak in the number of events (around $m-2.0$) representing the sensitivity of the seismic system (m_{min}). The blue line is the maximum likelihood fit of the data as modeled by Eq. 7. Depending on where $m_{min}$is selected, this can significantly overestimate the potential largest event.

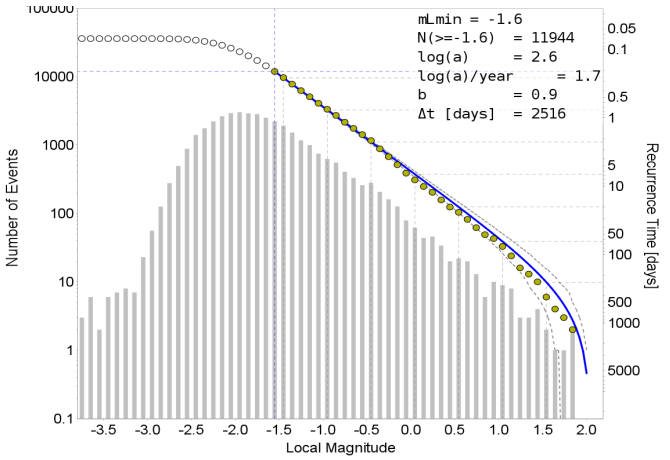

Fig. 4: Frequency-magnitude plot as per Fig. 3 except here the blue line represents an upper-truncated fit as given by Eq. 8 This is a more realistic measure of the occurrence of larger magnitude events in mining.

In mining, tools using temporal and spatial changes in b for short term seismic hazard assessment have been developed. The concern with this method is that the data selection, by its nature, reduces the amount of data available, which, in turn, increases the uncertainty in b. It is then difficult to separate changes in b with changes in stress or with uncertainties in fitting of the data. The frequency-magnitude distribution is also a statistical measure and so should only be used when there is enough data.

Another aspect of the frequency-magnitude distribution is recurrence times of larger seismic events. This is a probabilistic approach and should be used as such. For example, a recurrence time of one year does not mean there will be exactly one such event each year. It is also based on historic data, and so any future forecast makes the assumption that conditions, in the future, will be the same as the past.

With the limitation of the open-ended nature of Eq. 7, an upper truncated formulation was developed by Page (1968) and Cosentino et al. (1977):

$$N(\geq m) = 10^{a}(10^{-bm} - 10^{-bm_{max}}) \tag{8}$$

where $m_{max}$is the largest observed event. Fig. 4 shows the upper truncated fit to the same data set as shown in Fig. 3. This doesn't have a significant effect on b, but does give a more realistic recurrence time for larger magnitude events.

One final word of caution when using the frequency-magnitude distribution graphs. It is tempting to use Eq. 7 with $N = 1$ to estimate the largest magnitude event as a/b. This is incorrect as Eq. 3 is scale invariant, meaning the probability of an event larger than a/b is not zero, even when the fit line matches the observed data for larger magnitudes. It is better to use other methods to estimate the largest magnitude event, such as record theory as proposed by Mendecki (2012).

4.7. Apparent Volume

Apparent volume, V_A, as defined in Eq. 9, is a model-independent parameter which describes the volume of rock which experiences coseismic inelastic deformation, resulting in radiated seismic waves from a seismic event.

$$V_A = \frac{\mu P^2}{2E} \tag{9}$$

where μ is rigidity , P is the seismic potency and E the radiated seismic energy. Plotting the cumulative V_A over time has the advantage over cumulative potency, or moment, of being less sensitive to the size of the event. This results in a smoother plot, with fewer sudden jumps, caused by larger seismic events, which may hide interesting details. It also highlights smaller events which may have resulted in larger than expected deformation (Fig. 5). A time history of cumulative V_A, plotted with sliding windows of Energy Index (discussed below), is shown in Fig. 10.

4.8. Apparent Stress

Although stress drop, $\triangle\sigma$, can be estimated from the basic source parameters, as follows:

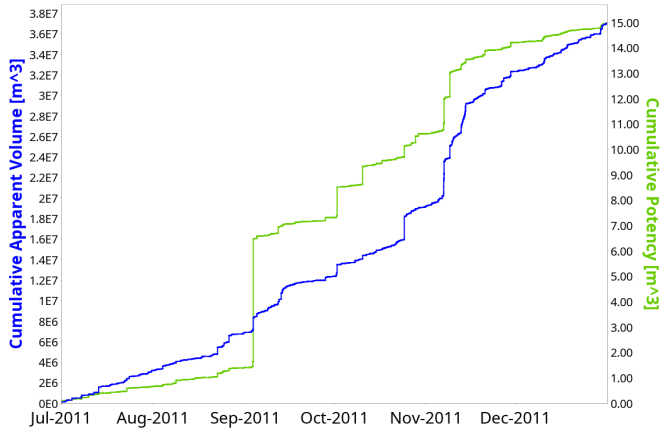

Fig. 5: Time history of cumulative V_A and cumulative P for a six month period. P is based purely on the size of the seismic events with jumps in P due to larger seismic events. Cumulative V_A is richer in detail, where deformation, even from smaller events, is easier to visualize.

$$\triangle\sigma = c_2 M f_0^3 \tag{10}$$

where c_2 is a constant ($\simeq 1.8 \times 10^{-10}$ for S-waves in hard rock), and M is the seismic moment. The cubic dependence on corner frequency, f_0, does mean that this is not a well-constrained parameter. Because of this, apparent stress:

$$\sigma_A = E/P \tag{11}$$

is generally a more stable measure of the stress change at the seismic source. Fig. 6 shows how apparent stress can vary in space. This is a useful tool in understanding the relative stress levels across a mine. One downside to apparent stress is that it does scale with the size of the event (Fig. 7), and so analysing events based on apparent stress, using events with different magnitudes will be biases by the magnitude of the events. Therefore events of similar magnitudes should be considered when using apparent stress.

4.9. Energy Index

A parameter which is less sensitive to magnitude but also conveys information about local stress conditions is Energy Index (EI) (Butler and van Aswegen, 1993). The concept, as shown in Fig. 8, is to look at an event of a given potency (or moment) and determine if this event radiated more or less seismic energy, compared with a collection of similarly sized (potency) events. The expected energy can be determined from a best fit line on a $logE$ vs $logP$ plot, as shown in Fig. 8. Events with energy above the line would have a higher than average shear stress at the location of the event, while events with energy below the line

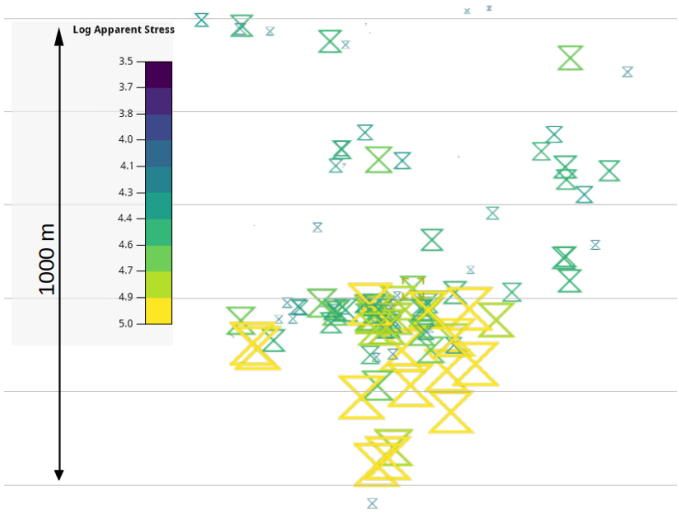

Fig. 6: Apparent stresses of selected seismic events with equal magnitudes (approximately $m+1.0$). The higher apparent stress events locate in the deeper section of the mine. The ratio of the highest to lowest apparent stress in this figure is nearly 100.

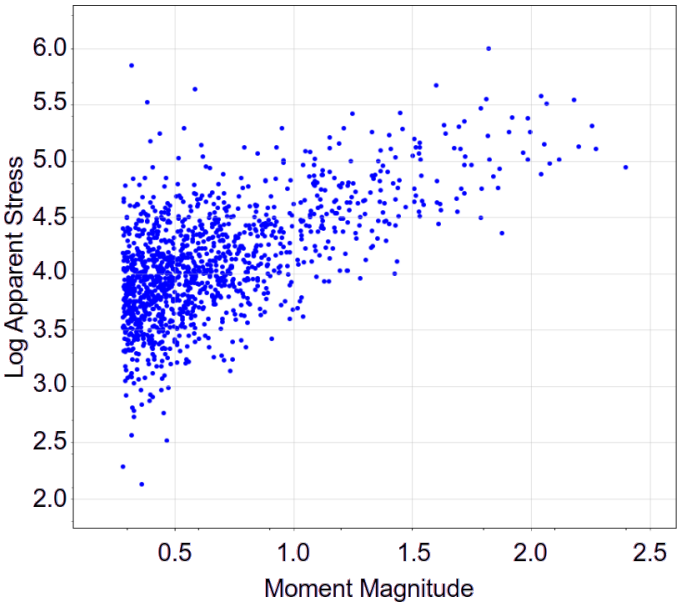

Fig. 7: Apparent stress versus moment magnitude for larger events recorded at a mine. Apparent stress does have a dependency on the magnitude of the event.

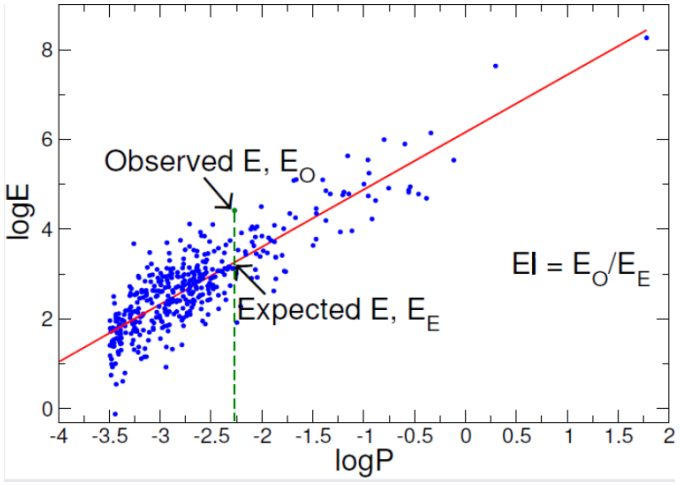

Fig. 8: A pictorial description of the concept of Energy Index (EI), where E is Energy and subscripts O, E indicate Observed and Expected (Butler and van Aswegen, 1993). A linear relation of the events in the $logE$ vs $logP$ allows for an expected value of the radiated energy, for a given potency, to be determined. If the observed energy of an event is above (or below) the line, the average shear stress at the source location would be higher (or lower) than average.

would have lower than average shear stress. While this does not give stress values, it is a good proxy for shear stress.

Fig. 9 shows an example of $logEI$ used in a spatial context. The events are coloured and sized by $logEI$ and show regions of higher or lower than average shear stress.

Another method where EI can be useful is to plot a time history of $logEI$ using a sliding window (Hills et al., 2013). This shows the temporal trend of shear stress. In this case, it is best to limit the events to a specific spatial region, such as a pillar or cluster of events. If too large a region is selected, the decrease of stress in one sub-region may result in an increase in stress in another sub-region. The result would be that the time history may only show an average over the whole region. Fig. 10, from Hills et al. (2013), shows an example of a rapid decrease in $logEI$ before a large seismic event. The success rates of such time history analysis, as a precursory indicator for large events, is not high, as reported by Hills et al. (2013). However, energy indexing can be used as an indicator of changing rock mass conditions.

4.10. Re-entry and short term seismic hazard

There are many tools currently being used for determining re-entry times after blasts or large magnitude seismic events. Almost all of these tools use some form of an event rate or energy rate approach. Modeling the decay rate using Omori's law is one of these tools, with Vallejos and McKinnon (2008) proposing practical guidelines.

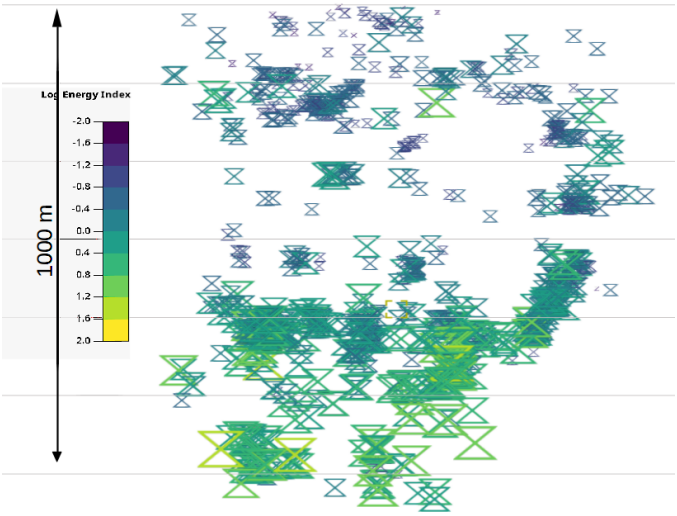

Fig. 9: A plot of events above $m - 1.0$ for the same mine as in Fig. 6. Here the events are sized and coloured by $logEI$. A similar trend of higher and lower stress regions are observed as shown in Fig. 6, but more events can be used. This allows for more of the space to be sampled.

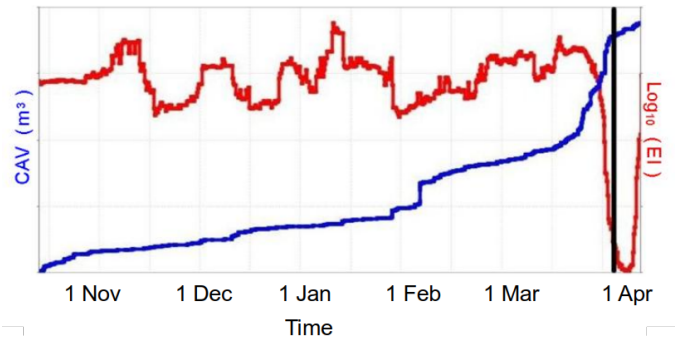

Fig. 10: A time history of $logEI$(red) and cumulative V_A(blue) for a four month period at Beaconsfield Mine, Australia. A sharp decrease in $logEI$ was observed from around the 28th of March 2008. Seismic deformation, as shown by the rapid increase in the cumulative V_A, also started around this time. This can be seen as larger strains occurring for a decrease in local stiffness. The mine was notified of a potential instability shortly after this (from Hills et al. 2013).

Even with these guidelines, these authors indicate that site specific calibration is required. As discussed above, responses to blasts and large magnitude events are dependent on local stress conditions. Therefore, calibration of the Omori parameters can be a continual process.

The Short Term Activity Tracker (STAT), discussed by Chester et al. (2018), is a probabilistic method of comparing the current activity rate with some reference rate, which can be calibrated for a mining region. This is an advance on a simple activity rate method in that it determines if there has been, say one event in the past 15 minutes, what is the likelihood of there being two events in the next hour, rather than waiting the full hour to count these. STAT is not only used for re-entry after a blast or large magnitude event, but can indicate when the short term seismic hazard has increased.

A more recent development in the short term seismic hazard field is to use ground motion alerts as proposed by Mendecki (2023). Since this uses ground motion, it is not limited to where seismic events locate, but can report on exposure of critical infrastructure to transient waves from mine wide seismicity.

5 SOURCE MECHANISM

5.1. Energy ratio (E_S/E_P)

The E_S/E_P ratio (S-wave energy over P-wave energy) is commonly used as a proxy for the source mechanism of a seismic event. Morkel et al. (2019) reviewed this ratio, as used in mine seismology, as well as identifying problems with the reliability of this parameter. Although, in theory, the E_S/E_P ratio is directly related to whether a source is implosive/explosive or shear, there are a few issues with how this is measured. The first issue is that estimating the radiated energy, especially for smaller events, is dependent on how much of the high frequency spectra is recovered and how well the attenuation of the high frequencies can be modeled. The second issue is when the seismic array consists of mostly uniaxial sensors, these sensors, at best, recover a third of the radiated energy. Furthermore, the orientation of the sensor element in relation to the direction of the source of the energy is an important factor in how much of each of the P- and S-wave energy the sensor element records. For example, specific areas of the mine may show events with artificially low E_S/E_P ratios, depending on the geometry and composition of the sensor array. This will lead to misinterpretation of the seismic data. Caution should be used when relying on E_S/E_P ratio, and where possible, actual source mechanisms should be used.

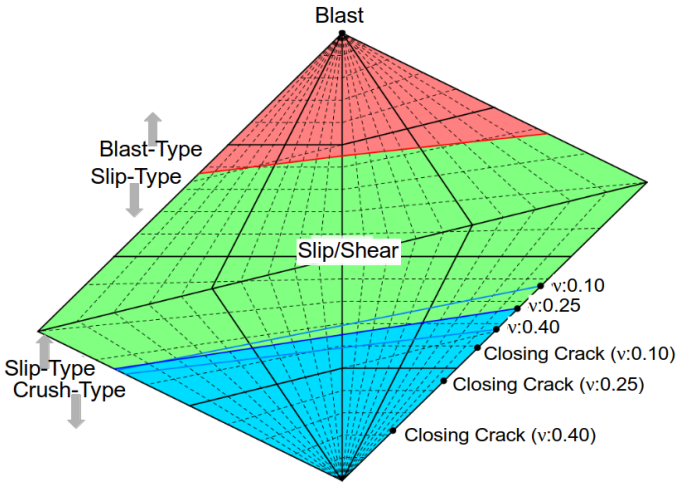

Fig. 11: Plot of source mechanism classifications as proposed by Hudson et al. (1989). The colouring of the regions has been added to identify the broad classifications, between crush and shear type sources.

5.2. Moment Tensor Inversion

The moment tensor of a seismic source is a general description of the source using a distribution of coupled dipoles to describe the inelastic deformation. This paper will focus on understanding the types of sources typically recorded in mining, rather than the theory of how moment tensors are calculated. For those interested, Madariaga (2015) discusses the theory of moment tensors, although mostly from an earthquake science perspective. In mining, there are two main types of source mechanisms (Ryder, 1988 and Malovichko, 2020). Blasts are excluded, as we are looking at mining induced seismicity. These two types are shear failures and crush type sources as shown in the Hudson plot (Hudson et al., 1989) in Fig. 11. The unusual shape of the plot is to give equal area to all moment tensor solutions. Crack-opening mechanisms, upper left section of the Hudson plot, are more common with hydrofracturing and are not common mechanisms in mine seismology. Since moment tensors are calculated from the lower frequencies, the limitations as mentioned for moment above apply here. Sensor array geometry is also important as the source should be surrounded by triaxial sensors to capture the radiation pattern, as shown in Fig. 1. Uniaxial sensors can be used for moment tensor inversion, but only in conjunction with a good spread of triaxial sensors. Accelerometers can also be used for the inversion, although the low frequency noise typical with these sensors is a limiting factor. For all these reasons, an array of triaxial geophones well spread around the seismic event will give the best results.

Moment tensor results can also be displayed as beach

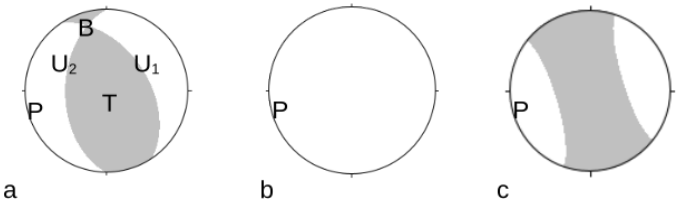

Fig. 12: Plot of source mechanisms, for three different sources, displayed as lower hemisphere projected beach balls. Picture (a) is of a purely shear event with the two potential slip planes indicated by U_1 and U_2. The labels P (maximum compressional deformation), B (intermediate or null axis), and T (minimum compressional deformation) indicate the orientations of the principal axes. Picture (b) is of a purely implosive source and (c) a typical crush type source. For these last to cases, only the P-axes have a physical meaning.

balls, as shown in Fig. 12. Examples of the three main source types are shown. The first is for a shear event, where the two nodal (slip) planes are indicated. The second is a purely implosive source and the third of a typical crush type source.

Shear type sources

Shear type sources are usually due to movement along a plane of weakness, such as a fault, dyke or contact. The beach ball representation in Fig. 12 (a) is the lower hemisphere projection of the compressional and tensional ground motions. The principal axes, P, B and T indicate the maximal, intermediate and minimal compressional directions. These are proxies for the local orientations of σ_1, σ_2 and σ_3 respectively. There are two slip planes, or nodal planes, indicated by $U_{1\&2}$. Moment tensor solutions of shear events will always give two orthogonal planes as the source is modeled as coupled dipoles. External information, such as geological mapping is needed to identify which of the two planes slipped. If these events locate away from excavations, the risk to excavations come from the transient seismic wave.

Crush type sources

These are seismic events close to excavations which result in the sudden bulking of the rockmass. This is caused by the compressional stress around the excavation which results in dynamic fracturing. The P-axis is approximately aligned with the direction of maximum compressional stress. Rigby (2023) suggest that this source is related to the elastic convergence of the surrounding rock mass rather than by rock fracturing. Only the P-axes are shown in Fig 12(b) and (c) as this is the only principal axis with a physical meaning for implosive and crush type sources. If a shear event occurs near an excavation, the resulting source mechanism is likely to be a combination of shear and crush type failure.

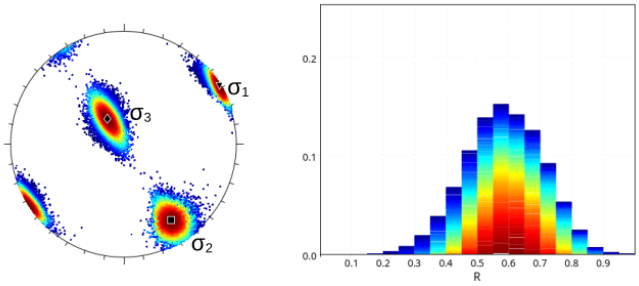

Fig. 13: Plot of stress inversion of seismic events, where source mechanisms with dominantly shear mechanism were used. The picture on the left is a stereonet showing the orientations of the principal stresses, while the plot on the right shows the distribution of stress magnitude ratios, R, for the given data set.

Finite Source Inversion

Larger seismic events may be quite complex, comprising multiple failures in rapid succession. It is possible to model these failures as a collection of point sources with different moment tensors and initiation times. The theoretical waveforms from the model are compared with the observed waveforms to confirm the validity of the modeled sources. The collection of modeled sources which match the observed waveforms may not be unique, but comparing these with underground observations can give insight into the complex failure (Malovichko, 2022).

6 STRESS INVERSION

When a set of moment tensor solutions are available, it is possible to invert the stress orientations which best match the observed slip from the source mechanisms. One, of a number of algorithms, which has been developed for this inversion process was developed by Michael (1984). It is important to note that only shear source mechanisms can be used for this inversion, and as Lundstern et al. (2024) point out, it is important to use data with a diversity of nodal plane orientations. What this means is, if all the source mechanisms are from slip on a particular fault, the inversion will not give an accurate picture of the local stress orientation.

Although it is not possible to obtain the absolute magnitudes of the stress, a stress magnitude ratio, R, can be obtained:

$$R = \frac{(\sigma_1 - \sigma_2)}{(\sigma_1 - \sigma_3)} \tag{12}$$

A large value of R indicates that σ_2 and σ_3 are of similar magnitude, while a low value of R indicates that σ_1 and σ_2 are of similar magnitude.

An example of the results of a stress inversion are shown in Fig 13. The R value, from Eq. 12 is around 0.6 in this example.

Stress inversion can help with calibrating a stress model for the mine ((Earl et al., 2015) and Rebuli et al., 2018), although it should be noted that the inverted stress orientations are the local stress orientations from the region where the seismic data is selected.

7 CONCLUSIONS

Seismic monitoring in mines is a powerful tool for understanding the rock mass response to mining. Seismic events are caused by stress changes in the rock mass and so are a good measure of when and where these changes occur. Besides event time and location, source parameters and failure mechanisms can be estimated from the recorded waveforms. Each piece of information can be used on its own, for example where the events are locating, the largest event recorded to-date, and the current activity rate. When the information is combined, more insight into the rock mass response can be gleaned. Combining location, timing and EI can show how the stress is changing in a particular region of the mine. Timing and ground motions can be used to understand short term hazard and re-entry.

Moment tensor analysis allows the failure mechanism to be understood. For example, smaller events can be used to identify potentially hazardous geological features before they become a problem. For larger, more complex, failures it is possible to combine multiple sub-sources to model the failure process. This can yield insight into the observed damage resulting from the larger event.

Stress inversion is a useful tool for calibrating stress models, but only when the appropriate data is used for the inversion.

With all of these analyses, the limitations of the measurements need to be understood. Otherwise incorrect conclusions can be drawn. This is just as true for seismic monitoring. Blindly inputting all the data to a software analysis package, will give results, but these results should be judiciously interpreted, or even discarded, while keeping the limitations in mind.

Although other seismic parameters have been proposed as analysis tools over the years, the ones discussed in this paper are the more commonly used, and useful parameters, in the author's opinion.

REFERENCES

1. Butler, A. G. and van Aswegen, G. (1993). Ground velocity relationships based on a large sample of underground measurements in two South African mining regions. In Young, R. P., editor, *Proceedings of the 3rd International Symposium on Rockbursts and Seismicity in Mines, Kingston, Ontario, Canada*, pages 41–50. Balkema, Rotterdam.

2. Chester, C., Cuello, D., and Basson, G. (2018). Development and implementation of the short term activity tracker and mine control trigger response system. In Potvin, Y. and Jakubec, J., editors, *Caving 2018: Proceedings of the Fourth International Symposium on Block and Sublevel Caving*, pages 521–532, Perth. Australian Centre for Geomechanics.

3. Cosentino, P., Ficarra, V., and Luzio, D. (1977). Truncated exponential frequency-magnitude relationship in earthquake statistics. *Bulletin of the Seismological Society of America*, 67(6):1615–1623.

4. Earl, P., Malovichko, D., and Rebuli, D. (2015). Study of stress conditions at williams mine using underground observations and microseismic monitoring data. In Potvin, Y., editor, *Design Methods 2015: Proceedings of the International Seminar on Design Methods in Underground Mining*, pages 149–163, Perth. Australian Centre for Geomechanics.

5. El-Isa, Z. and Eaton, D. W. (2014). Spatiotemporal variations in the b-value of earthquake magnitude-frequency distributions: Classification and causes. *Tectonophysics*, 615-616:1–11.

6. El-Isa, Z. H. (2018). Frequency-magnitude distribution of earthquakes. In Svalova, V., editor, *Earthquakes*, chapter 6. IntechOpen, Rijeka.

7. Gutenberg, B. and Richter, C. F. (1944). Frequency of earthquakes in California. *Bulletin of the Seismological Society of America*, 34:185–188.

8. Hanks, T. C. and Kanamori, H. (1979). A moment magnitude scale. *Journal of Geophysical Research*, 84:2348–2350.

9. Hills, P. B., Rebuli, D. B., and Lynch, R. A. (2013). Microseismic monitoring at the Tasmania mine, Beaconsfield, Tasmania. In Malovichko, A. and Malovichko, D., editors, *8th International Symposium on Rockbursts and Seismicity in Mines*, pages 485–494. Geophysical Survey of Russian Academy of Sciences.

10. Hudson, J. A., Pearce, R. G., and Rogers, R. M. (1989). Source type plot for inversion of the moment tensor. *Journal of Geophysical Research*, 94(B1):765–774.

11. Kaiser, P., McCreath, D., Tannant, D., laurentienne de Sudbury. Geomechanics Research Centre, U., and Program, C. R. R. (1996). *Canadian Rockburst Support Handbook*. Geomechanics Research Center.

12. Kanamori, H. (1972). Determination of effective tectonic stress associated with earthquake faulting. The Tottori earthquake of 1943. *Physics of the Earth and Planetary Interiors*, 5:426–434.

13. Lundstern, J.-E., Beauce, E., and Teran, O. J. (2024). The importance of nodal plane orientation diversity for earthquake focal mechanism stress inversions. *Geological Society, London, Special Publications*, 546(1):SP546–2023–63.

14. Madariaga, R. (2015). *Seismic Source Theory*, chapter 4, pages 51–71. Treatise on Geophysics: Second Edition.

15. Malovichko, D. (2020). Description of seismic sources in underground mines: Theory. *Bulletin of the Seismological Society of America*, 110:2124â2137.

16. Malovichko, D. (2022). Keynote: Utility of seismic source mechanisms in mining.

17. Martinsson, J. (2012). Robust Bayesian hypocentre and uncertainty region estimation: the effect of heavy-tailed distributions and prior information in cases with poor, inconsistent and insufficient arrival times. *Geophysical Journal International*, 192(3):1156–1178.

18. Mendecki, A. (2012). Size distribution of seismic events in mines. In *Australian Earthquake Engineering Society 2012 Conference, Dec 7-9, Queensland, Keynote Lecture*.

19. Mendecki, A. (2013). Frequency range, loge, log p and magnitude. In *Proceedings 8th International Symposium on Rockbursts and Seismicity in Mines, St Petersburg-Moscow, Russia Volume: 1*.

20. Mendecki, A. J. (2023). Seismic ground motion alerts for mines. *Journal of Seismology*, 27:599–608.

21. Mendecki, A. J., van Aswegwn, G., and Mountfort, P. (1999). A guide to routine seismic monitoring in mines. In Jager, A. J. and Ryder, J. A., editors, *A Handbook on Rock Engineering Practice for Tabular Hard Rock Mines*, chapter 9, pages 287–309. The Safety in Mines Research Advisory Committee, Johannesburg.

22. Meyer, S., Reading, A., and Bassom, A. (2022). The use of weighted self-organizing maps to interrogate large seismic data sets. *Geophysical Journal International*, 231(3):2156–2172. https://doi.org/10.1093/gji/ggac322.

23. Michael, A. J. (1984). Determination of stress from slip data: faults and folds. *Journal of Geophysical Research*, 89(B13):11517–11526.

24. Morkel, I., Wesseloo, J., and Potvin, Y. (2019). The validity of es/ep as a source parameter in mining seismology. In W, J., editor, *Deep Mining 2019: Proceedings of the Ninth International Conference on Deep and High Stress Mining*, pages 385–398, Johannesburg. The Southern African Institute of Mining and Metallurgy.

25. Mountfort, P. and Mendecki, A. J. (1997). Seismic transducers. In Mendecki, A. J., editor, *Seismic Monitoring in Mines*, chapter 1, pages 1–20. Chapman and Hall, London, 1 edition.

26. Omori, F. (1894). On the aftershocks of earthquakes. *J. Coll. Sci. Imperial University of Tokyo*, 7:111–200.

27. Page, R. (1968). Aftershocks and microaftershocks of the great Alaska earthquake of 1964. *Bulletin of the Seismological Society of America*, 58(3):1131–1168.

28. Rebuli, D., Goldswain, G., and Lynch, R. (2017). High quality microseismic monitoring in mines: Accelerometers or geophones? In Vallejos, J. A., editor, *Proceedings of the Ninth International Symposium on Rockbursts and Seismicity in Mines*, pages 23–31, Santiago, Chile.

29. Rebuli, D. B., Malovichko, D., and Conley, A. (2018). Seismic Calibration of in Situ Stress at Williams Mine. volume All Days of *U.S. Rock Mechanics/Geomechanics Symposium*, pages ARMA–2018–864.

30. Richter, C. F. (1935). An instrumental earthquake magnitude scale. *Bulletin of the Seismological Society of America*, 25:1–32.

31. Rigby, A. (2023). Physically motivated moment-tensor decomposition for mining-induced seismicity. *Geophysical Journal International*, 236(1):443–455.

32. Ryder, J. (1988). Excess shear stress in the assessment of geologically haz-ardous situations. *J. South. Afr. Inst. Min. Metall*, 88(1):27–39.

33. Sonley, E. and Atkinson, G. M. (2005). Empirical relationship between moment magnitude and Nuttli magnitude for small-magnitude earthquakes in Southeastern Canada. *Seismological Research Letters*, 76(6):752–755.

34. Utsu, T. (1961). A statistical study on the occurrence of aftershocks. *Geophysical Magazine*, 30:521–605.

35. Vallejos, J. and McKinnon, S. (2008). Guidelines for development of re-entry protocols in seismically active mines. *42nd U.S. Rock Mechanics - 2nd U.S.-Canada Rock Mechanics Symposium*.

36. Zheng, X., Sun, J., Yao, L., Liu, L., and Shao, A. (2018). A three-dimensional oblique incidence method based on stress time-history functions of seismic body waves. *Environmental Earth Sciences*, 77:528.